Korean J Pain 2022;35(3):250-260
https://doi.org/10.3344/kjp.2022.35.3.250
pISSN 2005-9159 eISSN 2093-0569

KJP

Experimental Research Article

Check for updates

Identification of cranial nerve ganglia using sectioned images and three-dimensional models of a cadaver

Chung Yoh Kim[1], Jin Seo Park[1], and Beom Sun Chung[2]

[1]*Department of Anatomy, Dongguk University School of Medicine, Gyeongju, Korea*
[2]*Department of Anatomy, Yonsei University Wonju College of Medicine, Wonju, Korea*

Received January 12, 2022
Revised April 2, 2022
Accepted April 6, 2022

Handling Editor: Yeon-Dong Kim

Correspondence
Beom Sun Chung
Department of Anatomy, Yonsei University Wonju College of Medicine, 20 Ilsan-ro, Wonju 26426, Korea
Tel: +82-33-741-0272
Fax: +82-33-742-1434
E-mail: bschung@yonsei.ac.kr

Previous presentation at conference:
This article was presented at the Annual Meeting of Korean Association of Anatomists on October 14, 2021, in Jeju.

Background: Cranial nerve ganglia, which are prone to viral infections and tumors, are located deep in the head, so their detailed anatomy is difficult to understand using conventional cadaver dissection. For locating the small ganglia in medical images, their sectional anatomy should be learned by medical students and doctors. The purpose of this study is to elucidate cranial ganglia anatomy using sectioned images and three-dimensional (3D) models of a cadaver.
Methods: One thousand two hundred and forty-six sectioned images of a male cadaver were examined to identify the cranial nerve ganglia. Using the real color sectioned images, real color volume model having a voxel size of 0.4 × 0.4 × 0.4 mm was produced.
Results: The sectioned images and 3D models can be downloaded for free from a webpage, anatomy.dongguk.ac.kr/ganglia. On the images and model, all the cranial nerve ganglia and their whole course were identified. In case of the facial nerve, the geniculate, pterygopalatine, and submandibular ganglia were clearly identified. In case of the glossopharyngeal nerve, the superior, inferior, and otic ganglia were found. Thanks to the high resolution and real color of the sectioned images and volume models, detailed observation of the ganglia was possible. Since the volume models can be cut both in orthogonal planes and oblique planes, advanced sectional anatomy of the ganglia can be explained concretely.
Conclusions: The sectioned images and 3D models will be helpful resources for understanding cranial nerve ganglia anatomy, for performing related surgical procedures.

Key Words: Anatomy, Cross-Sectional; Cadaver; Cranial Nerves; Dissection; Facial Nerve; Ganglia, Parasympathetic; Glossopharyngeal Nerve; Imaging, Three-Dimensional; Neuroanatomy.

INTRODUCTION

Cranial nerve ganglia can be damaged by neoplasms, viral infections, and even from surgical procedures targeting other organs; therefore, physicians should understand their detailed anatomy for accurate diagnosis and treatment. Knowledge of the sectional anatomy of the cranial nerve ganglia is needed for interpreting magnetic resonance imaging (MRI) and computed tomography (CT) images during diagnosis [1,2]. Moreover, their stereoscopic

Author contributions: Chung Yoh Kim: Writing/manuscript preparation; Jin Seo Park: Data curation; Beom Sun Chung: Supervision.

anatomy should be understood for performing surgeries and local anesthetic injections [3,4].

However, existing methods for learning the anatomy of the cranial nerve ganglia have several limitations. It is difficult to identify the cranial nerve ganglia during cadaver dissection because of their small size and the overlying muscles and bones. Photographs of skillfully dissected cadavers can show only fragmented views that are hardly related to orthogonal medical images or surgical views [5,6]. It is difficult for novices to understand the cranial nerve ganglia anatomy using MRI because it uses grayscale color and has low resolution (pixel size, 0.5 × 0.5 mm) [7].

Alternatively, sectioned images and three-dimensional (3D) models of cadavers can be used to elucidate the sectional anatomy and stereoscopic anatomy of the cranial nerve ganglia. Compared to MRI, sectioned images are in real color and have high resolution (pixel size, 0.06 × 0.06 mm) that can reveal even minute anatomical structures, including the cranial nerve ganglia. By 3D reconstruction, the sectioned images can be converted into surface models [8] and real color volume models [9] that can be utilized for virtual dissection and virtual surgery.

This study aimed to enhance the understanding of the anatomy of the cranial nerve ganglia using sectioned images and 3D models of a cadaver. All the cranial nerve ganglia and their detailed course were identified on the sectioned images, while their spatial relationships were elucidated using 3D models. The cadaver data could be a helpful resource for physicians who diagnose and treat cranial nerve ganglia diseases.

MATERIALS AND METHODS

A male cadaver whole body (height 1,765 mm, weight 46.0 kg) was frozen at –70°C for repeated sectioning and photography [10]. Among the resultant 3,512 sectioned images of the whole body, 1,246 images of the head region were chosen for this study. The images of the head region had a color depth of 48-bits, resolution of 8,688 × 5,792 pixels, pixel size of 0.06 × 0.06 mm, and interval of 0.2 mm [10,11]. This study was approved by the Institutional Review Board of Wonju Severance Christian Hospital (CR321181).

The first step was to identify all 12 pairs of the ganglia of the cranial nerves: the ciliary ganglion, trigeminal ganglion, pterygopalatine ganglion, otic ganglion, submandibular ganglion, geniculate ganglion, vestibular ganglion, spiral ganglion, superior and inferior glossopharyngeal ganglia, and superior and inferior vagal ganglia (**Table 1**) [12-23]. For this, sectioned images of the brainstem were examined to determine the origins of the cranial nerves (**Fig. 1A**). From the origins of the cranial nerves, the nerve fibers were tracked to identify the cranial nerve ganglia and related structures (**Fig. 1B**). Distinguishing landmarks, such as cranial foramina, were identified to confirm the locations of the cranial nerve ganglia (**Fig. 1C**). All cranial nerve ganglia and adjoining structures were examined by referring to neuroanatomy textbooks and research articles. The ganglia were segmented at 0.4-mm intervals using a software program (Adobe Photoshop CC 2018; Adobe Systems, Inc., San Jose, CA) [24] to produce the 3D models.

To produce the volume models of the whole head and cranial nerve ganglia, the sectioned images were resized and chosen to yield a pixel size of 0.4 × 0.4 mm and interval of 0.4 mm. The sectioned images in PNG format were converted to digital imaging and communications in medicine (DICOM) format using Adobe Photoshop CC 2018 and aligned using a DicomBrowser [25]. The DICOM files were 3D reconstructed using MRIcroGL (www.mccauslandcenter.sc.edu), including dcm2nii [26], and saved in a neuroimaging informatics technology initiative format. The resultant real color volume model had a voxel size of 0.4 × 0.4 × 0.4 mm [9].

To measure the sizes of all 12 pairs of the ganglia, the volume models of the ganglia were overlaid on the volume model of whole head in MRIcroGL. Based on the sectioned images and overlaid volume models, the margins of all ganglia were checked. Based on the coordinate data of the ganglia, their lengths, widths, and heights were calculated.

RESULTS

In the sectioned images of the orbit, cavernous sinus, internal acoustic meatus, pterygopalatine fossa, floor of the oral cavity, jugular foramen, and infratemporal fossa, 12 pairs of cranial nerve ganglia were identified and labeled (**Figs. 2**, **3**). A real color volume model of the male cadaveric head (voxel size, 0.4 × 0.4 × 0.4 mm; file size, 175 MB) and 12 overlay files of the cranial nerve ganglia (average file size, 668 KB each) were produced (**Fig. 4A**). The volume model could be cut in the orthogonal and oblique planes (**Fig. 4B**) in the MRIcroGL. The overlay files of the cranial nerve ganglia could be displayed together with the volume model of the whole head (**Fig. 4C**). The sectioned images in the original resolution and volume models have been uploaded to the authors' webpage (anatomy.dongguk.ac.kr/ganglia) to be downloaded.

1. Oculomotor nerve and ciliary ganglion

In the sectioned images, the oculomotor nerve emerged

Table 1. List of cranial nerve ganglia and their clinical features

Main cranial nerve	Ganglion	Clinical features
III Oculomotor nerve	Ciliary ganglion	The ciliary ganglion can be injured during surgical intervention such as lateral orbitotomy, inferolateral endoscopic orbital approach, transmaxillary approach to the orbit [12].
V Trigeminal nerve	Trigeminal ganglion	The trigeminal ganglion can be affected by herpes zoster virus infection [13]. To treat trigeminal neuralgia, trigeminal ganglion can be selected for radiofrequency selective ablation [13].
VII Facial nerve	Geniculate ganglion	The geniculate ganglion can be injured during surgical interventions such as the transmastoid approach, translabyrinthine approach, and middle cranial fossa approach due to abnormalities such as tumors [14].
	Pterygopalatine ganglion	To perform a pterygopalatine ganglion block, the intranasal approach, transoral approach, or infrazygomatic arch approach can be selected [15].
	Submandibular ganglion	To treat sialorrhea, the submandibular ganglion can be selected for injection of botulinum toxin A or surgical removal [16].
VIII Vestibulocochlear nerve	Spiral ganglion	To treat sensoneural hearing loss, studies to identify novel treatment to prevent and reverse the damage of spiral ganglion neurons including gene therapy and stem cell therapy [17].
	Vestibular ganglion	To treat vestibular schwannomas of the middle cranial fossa, the translabyrinthine, and retrosigmoid approaches can be selected [18].
IX Glossopharyngeal nerve	Superior ganglion (IX)	To treat glossopharyngeal neuralgia, percutaneous radiofrequency coagulation of nerves inside the jugular foramen can be selected [19].
	Inferior ganglion (IX)	To treat glossopharyngeal neuralgia, percutaneous radiofrequency coagulation of the inferior ganglion and nerves inside the jugular foramen can be selected [19].
	Otic ganglion	Frey's syndrome can occur by aberrant regeneration of cut parasympathetic fibers between the otic ganglion and subcutaneous vessels [20]. To treat trigeminal autonomic cephalalgias, the otic ganglion can be selected for injection of botulinum toxin A [21,22].
X Vagus nerve	Superior ganglion (X)	Vagal paraganglioma can originate from the superior ganglion of the vagus nerve [23].
	Inferior ganglion (X)	Vagal paraganglioma mostly originates from the inferior ganglion of the vagus nerve [23].

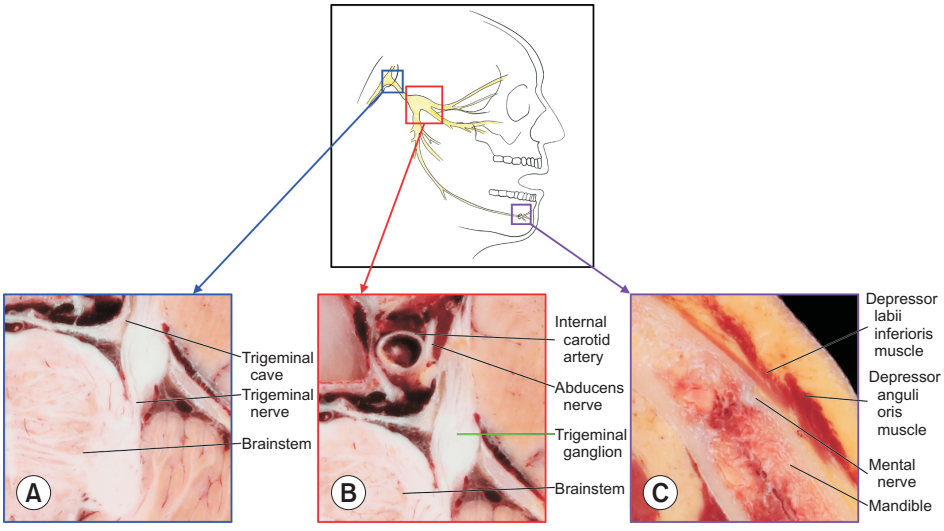

Fig. 1. Procedure to identify trigeminal ganglion in the horizontally sectioned images of a cadaver. To identify trigeminal ganglion, starting point (A) of the trigeminal nerve is observed in the sectioned images of brainstem. By tracking trigeminal nerve fibers, the ganglion (B) is observed. To confirm the location of the ganglion, ending point (C) of trigeminal nerve is observed.

from the interpeduncular fossa under the mammillary body. The nerve passed through the superior part of the cavernous sinus, lateral to the internal carotid artery. It entered the orbit through the superior orbital fissure and then divided into superior and inferior divisions. The inferior division of the oculomotor nerve formed a ciliary ganglion around the apex of the orbit (**Fig. 2A**, **Table 2**). Unlike the other parts of the oculomotor nerve, the ciliary ganglion showed an oval, flattened shape with a reddish color. The length, width, and height of ciliary ganglion were 3.62 mm, 1.80 mm, and 1.44 mm respectively. Similar to that seen in textbooks and previous studies, the lateral rectus muscle was observed lateral to the ganglion. The ophthalmic artery was observed superomedial to the ganglion, and the optic nerve was visible more superomedially [27]. In the sagittally sectioned volume model, the optic nerve

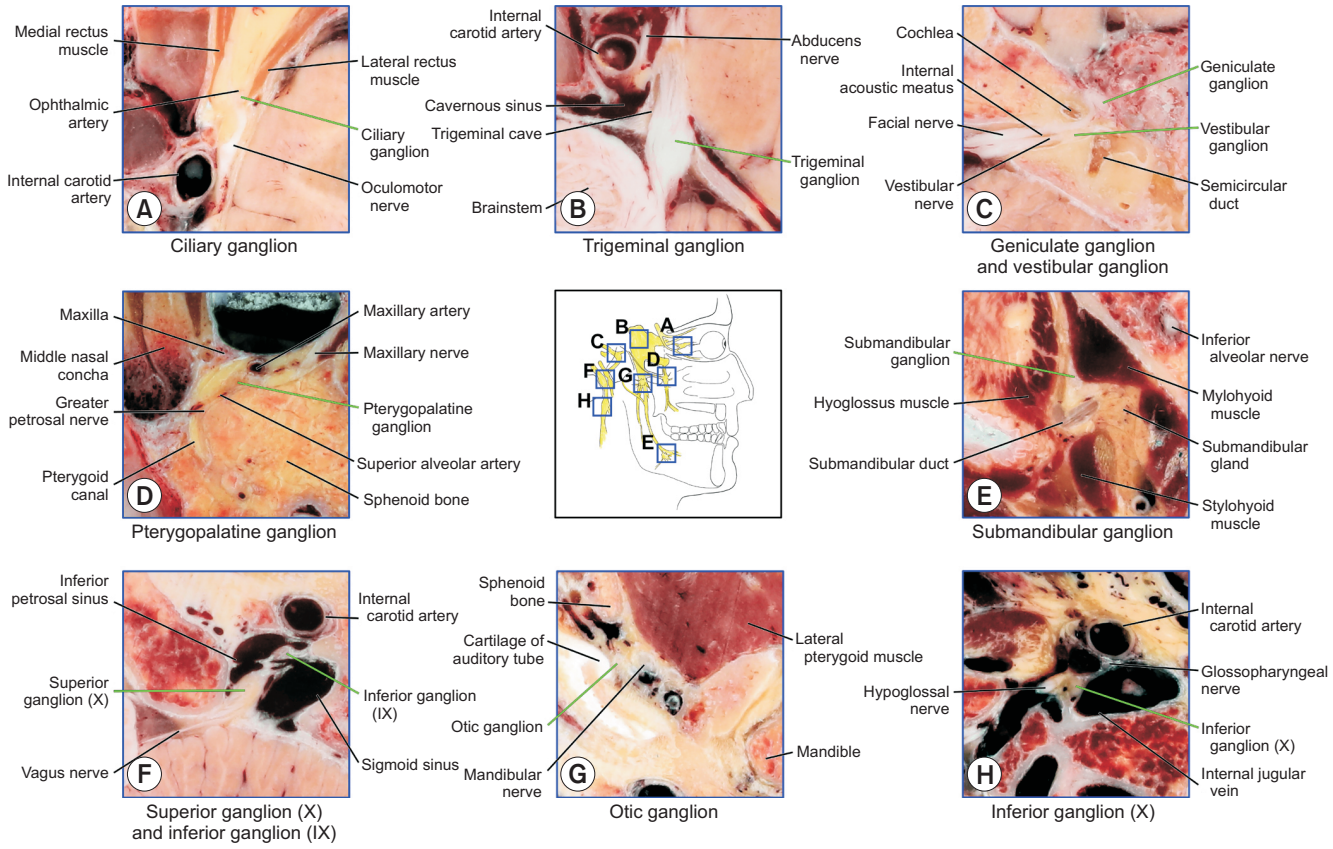

Fig. 2. Ten cranial nerve ganglia and adjacent structures identified in the horizontally sectioned images of a cadaver. Ten cranial nerve ganglia (A, ciliary ganglion; B, trigeminal ganglion; C, geniculate ganglion and vestibular ganglion; D, pterygopalatine ganglion; E, submandibular ganglion; F, superior ganglion of vagus nerve; G, otic ganglion; H, inferior ganglion of vagus nerve) and adjacent structures are identified and labeled in the sectioned images (IX, glossopharyngeal nerve; X, vagus nerve).

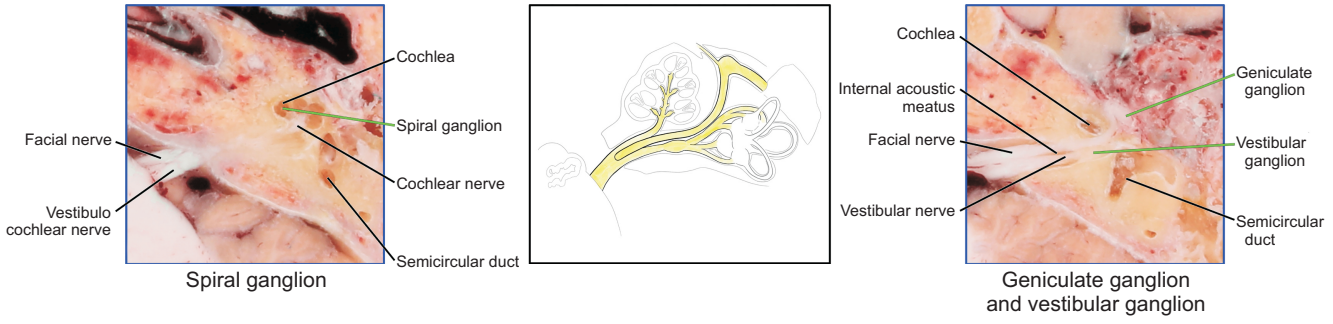

Fig. 3. Cranial nerve ganglia located near the internal acoustic meatus. Cranial nerve ganglia (A, spiral ganglion; B, geniculate ganglion and vestibular ganglion) and adjacent structures near the internal acoustic meatus and cochlea are identified and labeled in the sectioned images.

was observed superior to the ciliary ganglion, while the inferior rectus muscle was inferior to the ganglion. However, the ophthalmic artery could hardly be identified in the volume model because of its small size (**Fig. 5A**).

2. Trigeminal nerve and trigeminal ganglion

In the sectioned images, the trigeminal nerve emerged from the lateral aspect of the pons of the brainstem (**Fig. 1A**). It passed the pontocerebellar cistern and entered the middle cranial fossa through the porus trigeminus, thus corroborating with the existing literature [28]. The trigeminal ganglion was located near the posterolateral part of the cavernous sinus and lateral to the internal carotid artery and abducens nerve (**Fig. 2B**, **Table 2**). The trigeminal ganglion was semilunar shaped and shrouded in the dural recess called the trigeminal cave or Meckel's cave. The length, width, and height of trigeminal gan-

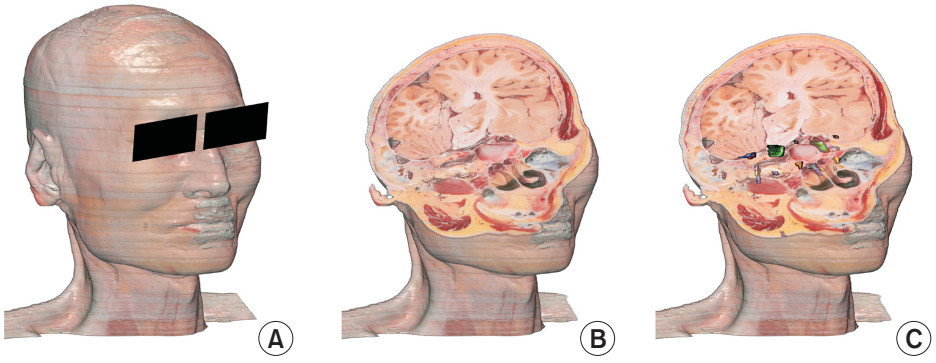

Fig. 4. Volume models of the whole head of a male cadaver and the cranial nerve ganglia. Real color volume model of the male cadaveric head (A) can be cut freely even in oblique plane (B). The overlay files of the cranial nerve ganglia can be displayed together with the volume model (C).

glion with the trigeminal plexus were 7.05 mm, 6.79 mm, 3.29 mm respectively. From the trigeminal ganglion, the three branches of the trigeminal nerve were identified and tracked: the ophthalmic, maxillary, and mandibular nerves. The ophthalmic nerve passed through the superior orbital fissure and supraorbital fissure. The maxillary nerve passed through the foramen rotundum and the infraorbital foramen. The mandibular nerve passed through the foramen ovale and divided into the lingual nerve and inferior alveolar nerve. The inferior alveolar nerve entered the mandibular canal through the mandibular foramen and eventually left the mandibular canal through the mental foramen (**Fig. 1C**). In the coronally sectioned volume model, the internal carotid artery and abducens nerve were identified superomedial to the trigeminal ganglion. The oculomotor nerve and trochlear nerve were identified superior to the ganglion (**Fig. 6A**).

3. Facial nerve ganglia

The sectioned images revealed that the facial nerve emerged from the junction of the pons and medulla oblongata, and then entered the internal acoustic meatus accompanying the vestibulocochlear nerve.

1) Geniculate ganglion

Near the fundus, which is the lateral end of the internal acoustic meatus, the geniculate ganglion was located lateral to the cochlea and anterior to the semicircular duct (**Fig. 2C**, **Table 2**), as reported in a previous study [29]. Because of the characteristic curvature of the facial nerve, the geniculate ganglion was easily identified. The length, width, and height of geniculate ganglion were 3.00 mm, 1.35 mm, and 1.74 mm respectively. From the geniculate ganglion, three nerve branches were identified. The first nerve branch passed through the stylomastoid foramen and was divided into branches to the facial nerve in the parotid gland. The greater petrosal nerve, the second branch, entered the pterygoid canal. The third branch, the chorda tympani nerve, passed the petrotympanic fissure and merged with the lingual nerve. In the coronally sectioned volume model, the facial nerve was observed passing through the internal acoustic meatus. The sharp bend of the geniculate ganglion was also visible. The cochlea and tympanic cavity were observed medial and lateral to the ganglion, respectively.

2) Pterygopalatine ganglion

The pterygopalatine ganglion was located posterosuperior to the maxillary sinus in the pterygopalatine fossa (**Fig. 2D**, **Table 2**). Unlike most parts of the nerve tract, the ganglion showed conical shape with reddish gray color [30], because it has a thinner myelin sheath than that of the other parts of the nerve tract. The length, width, and height of pterygopalatine ganglion were 2.41 mm, 2.40 mm, and 3.46 mm respectively. The greater petrosal nerve branch passed through the pterygoid canal and connected to the pterygopalatine ganglion (**Fig. 2D**). The sphenopalatine foramen was located superomedial to the pterygopalatine ganglion, but the nerve branches could not be distinguished. The nasopalatine nerve from the inferior aspect of the pterygopalatine ganglion reached the hard palate. The ganglion in the pterygopalatine fossa was observed in the sagittally sectioned volume model. The nasal cavity and maxillary sinus were observed anterior to the ganglion. Posteriorly, the sphenoid bone was visible, but unfortunately, the pterygoid canal could hardly be identified. Inferiorly, the medial pterygoid muscle could be observed (**Fig. 5B**).

3) Submandibular ganglion

The submandibular ganglion was located medial to the superior part of the submandibular gland (**Fig. 2E**, **Table 2**). The color of the ganglion was similar to that of the other parts of the nerve tract. However, it was slightly more swollen than the other parts. The length, width, and height of submandibular ganglion were 2.66 mm, 1.74 mm, and 3.63 mm respectively. The submandibular ganglion

Table 2. List of cranial nerve ganglia and their anatomical features observed in sectioned images

Main cranial nerve	Ganglion	Anatomical features					
		Location	Length[a] (mm)	Width[a] (mm)	Height[a] (mm)	Shape	Color
III Oculomotor nerve	Ciliary ganglion	In the orbital apex, medial to lateral rectus muscle, infralateral to optic nerve	3.62	1.80	1.44	Oval, flattened	Reddish
V Trigeminal nerve	Trigeminal ganglion	Near the posterolateral part of the cavernous sinus, lateral to the internal carotid artery and abducens nerve	7.05[b]	6.79[b]	3.29[b]	Semilunar	White
VII Facial nerve	Geniculate ganglion	Lateral to the cochlea, anterior to the semicircular duct, near the fundus of the internal acoustic meatus	3.00	1.35	1.74	Sharp bend	White
	Pterygopalatine ganglion	Posterosuperior to the maxillary sinus in the pterygopalatine fossa	2.41	2.40	3.46	Conical	Reddish gray
	Submandibular ganglion	Medial to the superior part of the submandibular gland	2.66	1.74	3.63	Swollen	White
VIII Vestibulocochlear nerve	Spiral ganglion	Near the lamina of the modiolus of the cochlea	NM[c]	NM[c]	NM[c]	Spot	Bright white
	Vestibular ganglion	Near the fundus of the internal acoustic meatus	1.17	3.14	1.00	Ampullated	Dark brown
IX Glossopharyngeal nerve	Superior ganglion	In the superior part of the jugular foramen, posterior to the inferior petrosal sinus	1.29	2.55	1.63	Expanded	Grayish orange
	Inferior ganglion	In the middle part of the jugular foramen, anterolateral to the superior ganglion (X), between the inferior petrosal sinus and sigmoid sinus	1.74	3.03	2.62	Expanded	Grayish orange
	Otic ganglion	Inferior to the foramen ovale, medial to the mandibular nerve, lateral to the cartilage of the auditory tube, anterior to the medial pterygoid muscle	2.08	1.82	1.84	Oval, small	White
X Vagus nerve	Superior ganglion	In the middle part of the jugular foramen, posterior to the inferior ganglion (IX)	5.61	3.07	3.32	Expanded	Bright yellow
	Inferior ganglion	Inferior to the jugular foramen, lateral to the hypoglossal nerve	2.81	3.55	6.64	Expanded	Dark brown

[a]Average of the left and right sides, [b]The lengths include the trigeminal plexus and trigeminal ganglion, [c]Not measurable, owing to its small size.

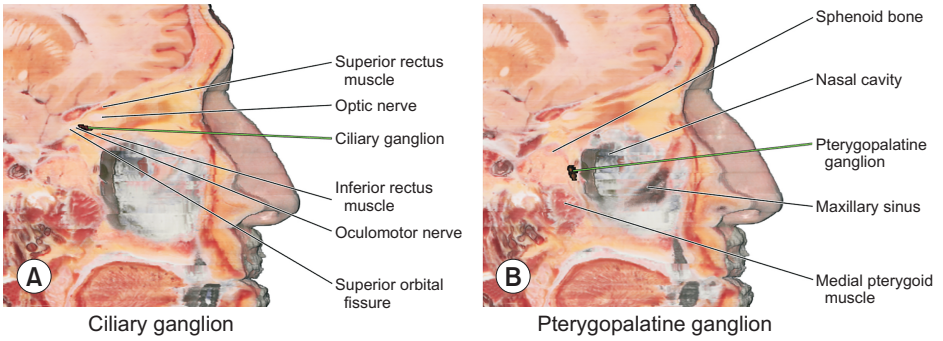

Fig. 5. Cranial nerve ganglia identified in the sagittal section of the volume model. The spatial relationships of the ciliary ganglion (A) and pterygopalatine ganglion (B) can be understood with adjacent structures in the sagittal section of the volume model.

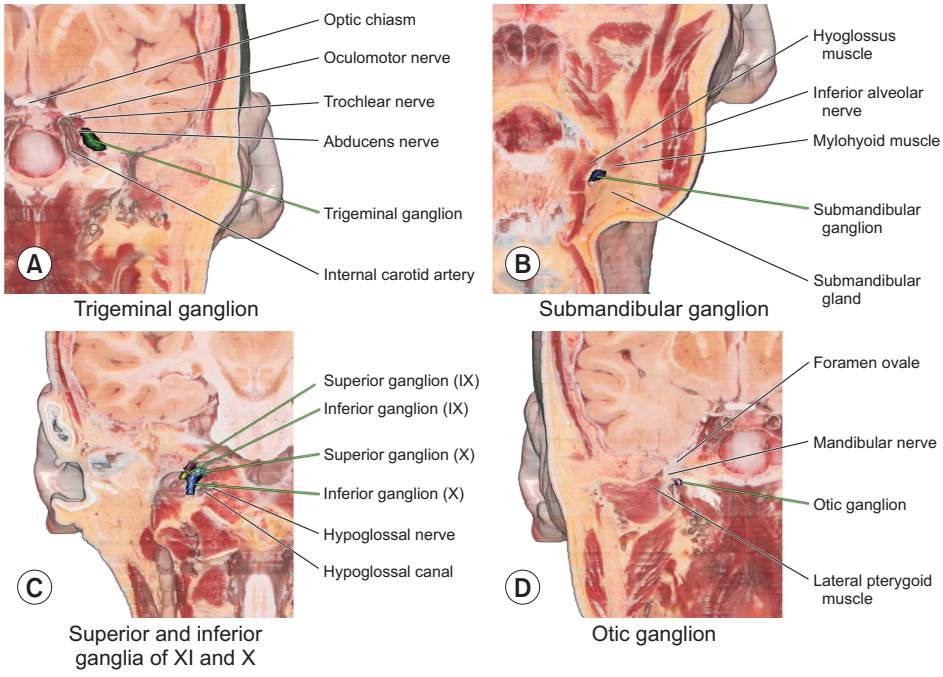

Fig. 6. Cranial nerve ganglia identified in the coronal section of the volume model (IX, glossopharyngeal nerve; X, vagus nerve). The spatial relationships of the cranial nerve ganglia (A, trigeminal ganglion; B, submandibular ganglion; C, superior and inferior ganglia of glossopharyngeal and vagus nerve; D, otic ganglion) can be understood with adjacent structures in the coronal section of the volume model.

was found in the lingual nerve tract on the posterior aspect of the mylohyoid muscle, similar to that shown in another study [16]. The lingual nerve was tracked in a reverse manner. The connection between the mandibular nerve and the chorda tympani nerve could be identified. The lingual nerve branch from the submandibular ganglion innervated the tongue and sublingual glands. Medial to the submandibular ganglion, the hyoglossus muscle was visible, as reported in another study [31]. In the coronally sectioned volume model, the ganglion could be observed with the adjacent structures. The submandibular gland was located inferior to the ganglion. The mylohyoid and inferior alveolar nerves in the mandible were observed lateral to the ganglion, while the hyoglossus muscle was medial to it (**Fig. 6B**).

4. Vestibulocochlear nerve ganglia

The origin of the vestibulocochlear nerve was the same as that of the facial nerve, but it was more on the lateral aspect of the junction of the pons and medulla oblongata. Similar to the facial nerve, the vestibulocochlear nerve reached the internal acoustic meatus in the sectioned images.

1) Spiral ganglion

The spiral ganglion was located in the modiolus of the cochlea (**Fig. 3A**, **Table 2**). The modiolus appeared dark brown in color in the sectioned images. In the modiolus, nerves having bright white color were observed. Near the lamina of the modiolus, the spiral ganglion was observed as a bright white spot. Because the lamina of the modiolus was visible, the cochlear nerve branch from the spiral ganglion could be identified, reaching the cochlea [32]. In the volume model, the ganglion was hardly identified because of its small size. However, since the cochlea was clearly visible, the location of the ganglion could be determined

using the volume model.

2) Vestibular ganglion

The vestibular ganglion was located near the fundus of the internal acoustic meatus (**Figs. 2C**, **3B**, **Table 2**). The ganglion was more ampullated, as reported in another study [33], and was darker than the other parts of the nerve. The length, width, and height of vestibular ganglion were 1.17 mm, 3.14 mm, and 1.00 mm respectively. Nerve branches from the vestibular ganglion reached the semicircular duct, lateral to the vestibular ganglion. In the coronally sectioned volume model, similar to the facial nerve, the vestibulocochlear nerve was seen passing through the internal acoustic meatus. The vestibular ganglion was visible at the end of the internal acoustic meatus.

5. Glossopharyngeal nerve ganglia

The sectioned images showed that the glossopharyngeal nerve emerged from the postolivary sulcus of the medulla oblongata and passed anterolaterally to leave the cranium through the jugular foramen.

1) Superior and inferior ganglia

The superior ganglion of the glossopharyngeal nerve was located in the superior part of the jugular foramen, posterior to the inferior petrosal sinus. The ganglion could be identified by its expanded shape and grayish orange color, unlike other parts of the nerve. The length, width, and height of superior ganglion were 1.29 mm, 2.55 mm, and 1.63 mm respectively. The inferior ganglion of the glossopharyngeal nerve was located in the middle part of the jugular foramen, anterolateral to the superior ganglion of the vagus nerve, and between the inferior petrosal sinus and sigmoid sinus (**Fig. 2F**, **Table 2**). Similar to the superior ganglion, the inferior ganglion of the glossopharyngeal nerve showed an expanded shape and grayish orange color. The length, width, and height of the inferior ganglion were 1.74 mm, 3.03 mm, and 2.62 mm, respectively. From the inferior ganglion of the glossopharyngeal nerve, the lingual branch emerged and reached the posterior part of the tongue. Below the jugular foramen, the glossopharyngeal nerve was narrow and had a white gray color. In the coronally sectioned volume model, the ganglia of the glossopharyngeal nerve were observed in the jugular foramen together with the ganglia of the vagus nerve. In the superior part of the jugular foramen, the superior ganglion of the glossopharyngeal nerve was identified. In the middle part of the jugular foramen, inferior to the superior ganglion of the glossopharyngeal nerve, the superior ganglion of the vagus nerve and inferior ganglion of the glossopharyngeal nerve were identified. In the inferior part of the jugular foramen, the inferior ganglion of the vagus nerve was identified. The hypoglossal nerve and hypoglossal canal were identified medial to the inferior ganglion of the vagus nerve (**Fig. 6C**).

2) Otic ganglion

The otic ganglion was found inferior to the foramen ovale (**Fig. 2G**, **Table 2**). The ganglion was located medial to the mandibular nerve, lateral to the cartilage of the auditory tube, and anterior to the medial pterygoid muscle, as mentioned in a previous study [6]. The otic ganglion was oval shaped with a white color, and was smaller than the mandibular nerve bundle. The length, width, and height of the otic ganglion were 2.08 mm, 1.82 mm, and 1.84 mm respectively. The auriculotemporal nerve branches emerged from the ganglion and reached the parotid gland. In the coronally sectioned volume model, the otic ganglion was observed with the adjacent structures. The auditory tube and its cartilage were observed medial to the ganglion. Laterally, the mandibular nerve appeared larger than the ganglion. The foramen ovale could be seen superior to the ganglion (**Fig. 6D**).

6. Vagus nerve ganglia

The vagus nerve emerged from the postolivary sulcus of the medulla oblongata, but medial to the glossopharyngeal nerve. The nerve entered the jugular foramen posterior to the glossopharyngeal nerve in the sectioned images.

1) Superior and inferior ganglia

The superior ganglion of the vagus nerve was found posterior to the inferior ganglion of the glossopharyngeal nerve (**Fig. 2F**, **Table 2**). The superior ganglion could be easily identified by virtue of its expanded shape and bright yellowish color. Also, several nerve fibers were visible in the superior ganglion. The main trunk of vagus nerve became narrow again after the superior ganglion. The length, width, and height of superior ganglion were 5.61 mm, 3.07 mm, and 3.32 mm respectively. Inferior to the jugular foramen and lateral to the hypoglossal nerve, the inferior ganglion could be identified with expanded shape and dark brown color (**Fig. 2H**, **Table 2**). The length, width, and height of inferior ganglion were 2.81 mm, 3.55 mm, and 6.64 mm respectively. From the inferior ganglion of the vagus nerve, the vagus nerve formed the superior cervical ganglion posterior to the internal carotid artery until the artery connected to the carotid sinus. The coronally

sectioned volume model showed a spatial relationship between the ganglia of the vagus nerve and those of the glossopharyngeal nerve (**Fig. 6C**). The inferior ganglion was larger than the superior ganglion, similar to that reported in a textbook [34].

DISCUSSION

The cranial nerve ganglia are deeply related to the parasympathetic and sensory functions of the head and neck region. Owing to this relationship, the ganglia are often selected as treatment targets (**Table 1**). For instance, the pterygopalatine ganglion and otic ganglion are blocked to control the pain caused by cluster headache [15,20,35–37]. Submandibular ganglion neurectomy can be performed using the transoral approach for treating sialorrhea [16]. Schwannomas affecting the vestibular ganglion or trigeminal ganglion can be surgically removed [18,38]. However, the clinical procedures and radiologic diagnosis of cranial nerve ganglia are difficult because their anatomy is highly complicated. For example, the interpretation of intraoperative fluoroscopy showing 2D projection requires detailed stereoscopic anatomy of the structures [15,35,36].

To understand the stereoscopic anatomy of the cranial nerve ganglia, the sectioned images and 3D models used in this study are more effective than the existing methods. The sectioned images provide realistic visualization of the ganglia and their surrounding structures, as their resolution and color are superior to those of MRI or CT (**Figs. 2**, **3**). Moreover, the volume model provides repetitive sectioning, unlike the conventional cadaver dissection. By observing the overlay file of the ganglion, the user can understand its spatial relationship with the surrounding tissues (**Figs. 4–6**).

The sectioned images and volume models of this study can elucidate the structures in the trajectory of ganglion nerve block procedure. As an example, to treat cluster headache, the pterygopalatine ganglion block can be performed owing to its proximity to multiple sensory facial and trigeminal branches. For the pterygopalatine ganglion block, the intranasal approach, infrazygomatic arch approach, and transoral approach can be chosen, but the nearby maxillary artery and maxillary nerve might be damaged [15]. The location and shape of the structures in the nerve block trajectory, including the artery and nerve, could be seen in detail in sectioned images, including **Fig. 2D**. Using the volume model that can be cut freely even in the oblique plane (**Figs. 4B**, **5B**), the nerve block trajectory can be thoroughly examined.

The sectioned images and 3D models of this study have the advantages of cadaver dissection and radiologic images. In cadaver dissections, anatomic structures can be observed in real colors and free viewing angles. In radiologic images, the internal structures can be observed without removing the overlying muscles and bones. The sectioned images and 3D models used in this study could provide real color and free viewing angles, as well as visualization of the surrounding structures of the cranial nerve ganglia. Due to these features, the pterygopalatine ganglion can be easily located on the sectioned images and 3D models. In the sectioned images, the pterygopalatine ganglion was displayed in real color, without loss of the overlying structures. Additionally, in the 3D models, the real color and adjacent structures of the pterygopalatine ganglion were observed in arbitrary sectioning planes (**Figs. 2**, **5**).

To identify the cranial nerve ganglia clearly, the sectioned images and 3D models were examined using the procedure described here. First, the entire course of each cranial nerve was inspected, including its origin, ganglion, and branches. Second, the appearance of the cranial nerve ganglia, including the size, shape, or color, was checked by referring to textbooks and previous research articles. Third, the spatial relationship between the cranial nerve ganglia and the adjacent structures was confirmed. This procedure followed for the sectioned images, and the 3D models corresponded to the identification procedure in conventional cadaver dissection.

The observations of this study can be compared to those of other studies. The locational descriptions of cranial nerve ganglia in this study corresponded to textbooks and other research. The shape and size description tended to follow aspects of other studies but was not exactly same. It is difficult for the shape descriptions to be exactly same because they largely depend on subjective viewpoints of the observers. Since there are various methods to observe cranial nerve ganglia, such as cadaver dissection, CT, MRI scans, or histological observations, it is difficult for the size to be exactly same. The color descriptions of previous studies were scarce in some ganglia that cannot be dissected easily. The advantage of this study was that the cranial nerve ganglia were observed in real color without formaldehyde fixation. The colors of ganglia in the sectioned images were different from other parts of the nerves, so we could identify the ganglia in the nerve tracks.

The limitation of this study is that only one cadaver was employed for the observation. This is because of the long time required for the cadaver sectioning. Most of other cadaver sectioned images are inadequate for the observation of minute ganglia, owing to their low resolution or artifacts [39]. For investigating differences in the cranial nerve ganglia between individuals, future studies using histologic or plastination specimens can be conducted.

Comparing dissection photographs with the sectioned images and 3D models of this study might provide a holistic viewpoint of the cranial ganglia. Clinical correlation using medical images and surgical photographs would increase the usefulness of this study.

In this study, the stereoscopic anatomy of the cranial nerve ganglia was elucidated using sectioned images and 3D models. By downloading the images and models from the authors' website (anatomy.dongguk.ac.kr/ganglia), medical students and doctors can virtually dissect the cadaver head to understand the spatial relationship of the deep head structures. The stereoscopic depiction of this study can be the foundation for clinical procedures, including neurectomy and radiologic diagnosis. In future studies, 3D models could be applied in 3D printing and virtual reality techniques for medical education and surgical training [39].

DATA AVAILABILITY

The datasets supporting the findings of this study are available from the corresponding author upon reasonable request.

CONFLICT OF INTEREST

No potential conflict of interest relevant to this article was reported.

FUNDING

This work was supported (in part) by the Yonsei University Wonju Campus Future-Leading Research Initiative of 2021 (2021-52-0057) and by the National Research Foundation of Korea (NRF) grant funded by the Korean government (MSIT) (No. 2021R1G1A1092673 and 2021R1F1A1063044).

ORCID

Chung Yoh Kim, https://orcid.org/0000-0001-8074-076X
Jin Seo Park, https://orcid.org/0000-0001-7956-4148
Beom Sun Chung, https://orcid.org/0000-0002-3644-9120

REFERENCES

1. Saremi F, Helmy M, Farzin S, Zee CS, Go JL. MRI of cranial nerve enhancement. AJR Am J Roentgenol 2005; 185: 1487-97.
2. VandeVyver V, Lemmerling M, Van Hecke W, Verstraete K. MRI findings of the normal and diseased trigeminal nerve ganglion and branches: a pictorial review. JBR-BTR 2007; 90: 272-7.
3. Khonsary SA, Ma Q, Villablanca P, Emerson J, Malkasian D. Clinical functional anatomy of the pterygopalatine ganglion, cephalgia and related dysautonomias: a review. Surg Neurol Int 2013; 4(Suppl 6): S422-8.
4. An JX, Liu H, Chen RW, Wang Y, Zhao WX, Eastwood D, et al. Computed tomography-guided percutaneous ozone injection of the Gasserian ganglion for the treatment of trigeminal neuralgia. J Pain Res 2018; 11: 255-63.
5. Rusu MC, Pop F, Curcă GC, Podoleanu L, Voinea LM. The pterygopalatine ganglion in humans: a morphological study. Ann Anat 2009; 191: 196-202.
6. Senger M, Stoffels HJ, Angelov DN. Topography, syntopy and morphology of the human otic ganglion: a cadaver study. Ann Anat 2014; 196: 327-35.
7. Bratbak DF, Folvik M, Nordgård S, Stovner LJ, Dodick DW, Matharu M, et al. Depicting the pterygopalatine ganglion on 3 Tesla magnetic resonance images. Surg Radiol Anat 2018; 40: 689-95.
8. Kim CY, Jung YW, Park JS. The Visible Korean: movable surface models of the hip joint. Surg Radiol Anat 2021; 43: 559-66.
9. Chung BS, Park JS. Real-color volume models made from real-color sectioned images of Visible Korean. J Korean Med Sci 2019; 34: e86.
10. You Y, Kim CY, Kim SK, Chung BS, Har D, Choi J, et al. Advanced-sectioned images obtained by microsectioning of the entire male body. Clin Anat 2022; 35: 79-86.
11. Park JS, Chung MS, Hwang SB, Lee YS, Har DH, Park HS. Visible Korean human: improved serially sectioned images of the entire body. IEEE Trans Med Imaging 2005; 24: 352-60.
12. Tesapirat L, Jariyakosol S, Chentanez V. Morphometric study of the ciliary ganglion and its pertinent intraorbital procedure. Folia Morphol (Warsz) 2020; 79: 438-44.
13. Moore KL, Dalley AF 2nd, Agur AM. Clinically oriented anatomy. 8th ed. Philadelphia, Lippincott Williams & Wilkins. 2018, pp 1956-7.
14. Hamzaoğlu V, Beger O, Erdoğan O, Kara E, Vayisoğlu Y, Taghipour P, et al. Radioanatomic assessment of the geniculate ganglion dehiscence and dimension: a cadaveric study. World Neurosurg 2020; 134: e913-9.
15. Piagkou M, Demesticha T, Troupis T, Vlasis K, Skandalakis P, Makri A, et al. The pterygopalatine ganglion and its role in various pain syndromes: from anatomy to clinical practice. Pain Pract 2012; 12: 399-412. Erratum in: Pain Pract 2012; 12: 673.
16. Spock T, Hoffman HT, Joshi AS. Transoral submandibular ganglion neurectomy: an anatomical feasibility study. Ann Otol Rhinol Laryngol 2015; 124: 341-4.

17. Zhang L, Chen S, Sun Y. Mechanism and prevention of spiral ganglion neuron degeneration in the cochlea. Front Cell Neurosci 2022; 15: 814891.
18. Guillotte A, Zand A, Ortiz M, Gan Y, Rivera A, Litofsky NS, et al. Clinical outcomes of resecting scarpa's ganglion during vestibular schwannoma surgery. J Clin Neurosci 2020; 76: 114-7.
19. Franzini A, Messina G, Franzini A, Marchetti M, Ferroli P, Fariselli L, et al. Treatments of glossopharyngeal neuralgia: towards standard procedures. Neurol Sci 2017; 38(Suppl 1): 51-5.
20. de Bree R, van der Waal I, Leemans CR. Management of Frey syndrome. Head Neck 2007; 29: 773-8.
21. Crespi J, Bratbak D, Dodick DW, Matharu MS, Senger M, Angelov DN, et al. Anatomical landmarks for localizing the otic ganglion: a possible new treatment target for headache disorders. Cephalalgia Rep 2019. doi: 10.1177/2515816319850761.
22. Crespi J, Bratbak D, Dodick DW, Matharu M, Solheim O, Gulati S, et al. Open-label, multi-dose, pilot safety study of injection of onabotulinumtoxinA toward the otic ganglion for the treatment of intractable chronic cluster headache. Headache 2020; 60: 1632-43.
23. Miller RB, Boon MS, Atkins JP, Lowry LD. Vagal paraganglioma: the Jefferson experience. Otolaryngol Head Neck Surg 2000; 122: 482-7.
24. Park JS, Chung MS, Hwang SB, Lee YS, Har DH. Technical report on semiautomatic segmentation using the Adobe Photoshop. J Digit Imaging 2005; 18: 333-43.
25. Archie KA, Marcus DS. DicomBrowser: software for viewing and modifying DICOM metadata. J Digit Imaging 2012; 25: 635-45.
26. Li X, Morgan PS, Ashburner J, Smith J, Rorden C. The first step for neuroimaging data analysis: DICOM to NIfTI conversion. J Neurosci Methods 2016; 264: 47-56.
27. Sinnreich Z, Nathan H. The ciliary ganglion in man (anatomical observations). Anat Anz 1981; 150: 287-97.
28. Tubbs RS, Mortazavi MM, Krishnamurthy S, Verma K, Griessenauer CJ, Cohen-Gadol AA. The relationship between the superior petrosal sinus and the porus trigeminus: an anatomical study. J Neurosurg 2013; 119: 1221-5.
29. Lan MY, Shiao JY. Using greater superficial petrosal nerve and geniculate ganglion as the only two landmarks for identifying internal auditory canal in middle fossa approach. Eur Arch Otorhinolaryngol 2010; 267: 1867-71.
30. Rong Z, Zixiang Y, Chang L, Guoxing X, Sheng Z, Yuanteng X, et al. Lacrimal hyposecretion: a surgical complication of juvenile nasopharyngeal angiofibroma. Am J Otolaryngol 2008; 29: 367-71.
31. Siéssere S, Vitti M, Sousa LG, Semprini M, Iyomasa MM, Regalo SC. Anatomic variation of cranial parasympathetic ganglia. Braz Oral Res 2008; 22: 101-5.
32. Mei X, Glueckert R, Schrott-Fischer A, Li H, Ladak HM, Agrawal SK, et al. Vascular supply of the human spiral ganglion: novel three-dimensional analysis using synchrotron phase-contrast imaging and histology. Sci Rep 2020; 10: 5877. Erratum in: Sci Rep 2020; 10: 7681.
33. Wu YW, Karandikar A, Goh JP, Tan TY. Imaging features differentiating vestibular ganglion from intracanalicular schwannoma on single-sequence non-contrast magnetic resonance imaging study. Ann Acad Med Singap 2020; 49: 65-71.
34. Mancall EL, Brock DG. Cervical plexus. In: Gray's clinical neuroanatomy: the anatomic basis for clinical neuroscience. Edited by Mancall EL, Brock DG. Philadelphia, Elsevier Health Sciences. 2011, pp 315-7.
35. Tepper SJ, Caparso A. Sphenopalatine ganglion (SPG): stimulation mechanism, safety, and efficacy. Headache 2017; 57 Suppl 1: 14-28.
36. Tolba R, Weiss AL, Denis DJ. Sphenopalatine ganglion block and radiofrequency ablation: technical notes and efficacy. Ochsner J 2019; 19: 32-7.
37. Crespi J, Bratbak D, Dodick D, Matharu M, Jamtøy KA, Tronvik E. Prediction of the sphenopalatine ganglion localization in computerized tomography images. Cephalalgia Rep 2019. doi: 10.1177/2515816318824690.
38. Song MH, Lee HY, Jeon JS, Lee JD, Lee HK, Lee WS. Jugular foramen schwannoma: analysis on its origin and location. Otol Neurotol 2008; 29: 387-91.
39. Roh TH, Oh JW, Jang CK, Choi S, Kim EH, Hong CK, et al. Virtual dissection of the real brain: integration of photographic 3D models into virtual reality and its effect on neurosurgical resident education. Neurosurg Focus 2021; 51: E16.